Spatial Phase Coherence in Femtosecond Coherent Raman Scattering

Ali Hosseinnia,[1,2,*] Michele Marrocco,[3,†] Francesco Vergari,[3,4] Meena Raveesh,[5] Sebastian Riewer,[1] Ashutosh Jena,[1] Abhishek Kushwaha,[1] Francesco Mazza,[1] Mark Linne,[6] Joakim Bood,[5] and Isaac Boxx[1]

[1]*Chair of Optical Diagnostics in Energy, Process and Chemical Engineering, RWTH Aachen University, 52062 Aachen, Germany*

[2]*Luxembourg Institute of Science and Technology, L-4422 Belvaux, Luxembourg*

[3]*ENEA, via Anguillarese 301, Roma I-00123, Italy*

[4]*Dipartimento di Fisica, Università di Roma "La Sapienza," Roma I-00185, Italy*

[5]*Division of Combustion Physics, Department of Physics, Lund University, S-221 00 Lund, Sweden*

[6]*School of Engineering, The University of Edinburgh, Edinburgh EH8 3JL, Scotland, United Kingdom*

(Received 7 February 2025; revised 11 June 2025; accepted 17 March 2026; published 22 April 2026)

Conventional femtosecond coherent laser spectroscopy predominantly focuses on the temporal phase coherence through time- or frequency-resolved methods. In this Letter, we suggest an alternative experimental framework based on spatial phase coherence. The intrinsic spectral dispersion of wave vectors in femtosecond pulses and sample dimensions exceeding the laser wavelength creates a compelling basis to establish spatial phase coherence as a novel approach to femtosecond laser spectroscopy. Using rotational Raman coherence in air as a case study, we analyze the transverse spatial distribution of the third-order signal generated by the rotational wave packet. Our findings reveal apparent temporal shifts and distortions in time-resolved signals that arise in conventional measurements lacking sensitivity to spatial phase coherence. Moreover, we demonstrate that spatial phase coherence can serve as a useful tool for thermometric applications, showcasing its sensitivity to temperature variations. These discoveries open new avenues in femtosecond laser spectroscopy, including an alternative single-shot detection scheme, a new form of Raman coherence imaging, and molecular species quantification during overlapping fractional revivals.

DOI: 10.1103/r98z-7bwj

Phase coherence is a cornerstone of collective phenomena, underpinning many remarkable advancements in both classical and quantum physics [1–7]. In laser spectroscopy, phase coherence is used in time- and frequency-resolved approaches or their combination, enabling insights into applications of atomic, molecular, and optical physics [8–11]. Beyond these conventional schemes, phase coherence is more comprehensively described in the framework of space-time four-vectors $(ct, \boldsymbol{r})$ and their reciprocal space duals $(\omega/c, -\boldsymbol{k})$. The more general context dictates that the temporal phase term ωt is complemented by the spatial term $-\boldsymbol{k}\cdot\boldsymbol{r}$. The link between spatial coordinates and wave vectors highlights the broader utility of phase coherence, extending its applications beyond traditional time- or/and frequency-resolved methods of laser spectroscopy. Examples are known in other branches of physics, such as stellar interferometry [12] or Bose-Einstein condensation [13]. From this perspective, spatial phase coherence offers a complementary avenue for spectroscopic investigations.

In this Letter, we investigate experimentally the spatial component of the signal's phase in relation to its temporal counterpart. Our aim is to explore the potential of space-wave vector coupling as a foundation for a new experimental platform designed to achieve a deeper understanding of phase invariance in ultrafast coherent laser spectroscopies. Additionally, we seek to define the influence of the spatial phase component on temporal phase information.

This research employs the framework of coherent Raman scattering (CRS) [9–11,14–19]. In this context, physical information is routinely gained under the assumption of localized interactions (i.e., uncorrelated temporal and spatial degrees of freedom limited to the propagation direction of the laser fields), as described by conventional response theories based on either third-order susceptibility [9,10] or anisotropic refractive index contributions [20] arising from molecular alignment [21]. The assumption allows us to neglect transverse spatial variations of the laser fields, and, under this approximation, the time-resolved homodyne signal in the impulsive regime, S_{ICRS}, is expressed as a time integral of the scattered field $E_S(t,\tau)$ at a fixed probe delay τ [9,16,17,20]

*Contact author: ali.hosseinnia@list.lu

†Contact author: michele.marrocco@enea.it

$$S_{\mathrm{ICRS}}(\tau) \propto \int dt |E_S(t,\tau)|^2. \tag{1}$$

Here, the scattered field is proportional to the macroscopic polarization $P_S(t,\tau)$ that depends on the temporal overlap of the two initial pulses that excite the Raman coherence, which is generated by a multitude of Raman transitions via combinations of spectral components of the two initial laser pulses.

In our approach (see Supplemental Material [22]), the transverse spatial components of the macroscopic polarization are considered. When expressed using modulated plane waves, these components drive the growth of the slowly varying scattered field amplitude $E(\boldsymbol{r},\omega)$ through the coupled Maxwell-Liouville equations [9,10]. Within this semiclassical picture, the fields are treated as classical c numbers, and $E(\boldsymbol{r},\omega)$ satisfies

$$\nabla^2 E(\boldsymbol{r},\omega) + 2i\mathbf{k}_S \cdot \boldsymbol{\nabla} E(\boldsymbol{r},\omega) = -\frac{\omega^2}{c^2} \sum_{m,n} d_n^m(\boldsymbol{r},\omega) e^{-\Gamma_n^m \tau} e^{i(\Delta\mathbf{k}\cdot\boldsymbol{r} + \Omega_n^m \tau)}, \tag{2}$$

where $\mathbf{k}_S$ is the scattered wave vector, $\Delta\mathbf{k}$ is the wave vector mismatch between scattered and incident laser fields, and indices m and n run over the molecular species and the Raman transitions. In the summation, the term $d_n^m(\boldsymbol{r},\omega)$ blends together the quantum-mechanical details of the Raman transitions, the spatial dependences of the laser pulses, and the spectral lines. In addition, the first exponential describes the field decay at the rate Γ_n^m due to the dephasing of the Raman coherence, while the phase factor reflects the Raman shift Ω_n^m and the spatial phase. Notice that Eq. (2) introduces the key point of this Letter: the slowly varying scattered field is highly sensitive to the phase $\Delta\mathbf{k}\cdot\boldsymbol{r} + \Omega_n^m\tau$. In the following considerations, we assume integrations over the longitudinal coordinate (z axis) and the spectral variables. The longitudinal integration contributes to phase matching, while leaving the transverse directions (x and y) available for detection of spatial phase effects. Spectral integration accounts for the convolution between the spectral dispersion of the Raman response and that of the laser pulses. Importantly, at the center of the transverse plane ($x = y = 0$), Eq. (2) simplifies to the conventional description of the scattered field. In this limit, the signal $S_{\mathrm{ICRS}}(\tau)$ of Eq. (1) is recovered. The correspondence with the conventional time-resolved signal $S_{\mathrm{ICRS}}(\tau)$ provides us with a simple description of the 2D homodyne signal visualized across the transverse (x,y) plane. In effect, the measured signal is factorized into a spatial term $G(x,y)$, which accounts for the spatial overlap of the laser pulses, and a temporal term that reproduces the impulsive time-resolved signal of Eq. (1):

$$S_{2D}(x,y,\tau) \propto G(x,y) S_{\mathrm{ICRS}}(\tau_{sp}). \tag{3}$$

In this expression, $\tau_{sp} = \tau + \Delta\tau$ introduces the concept of a spatial delay $\Delta\tau = a_x x + a_y y$ as emerging from the accumulated phase terms of Eq. (2) after longitudinal integration. Thus, the parameters a_x and a_y translate a spatial distance into the temporal separation $\Delta\tau$ at a fixed probe delay τ. Note that τ_{sp} reduces to the ordinary delay τ at the center of the transverse plane. Away from the center, the coefficients a_x and a_y encode phase invariance and the cumulative effect of multiple Raman transitions, each contributing a distinct frequency component to the generated wave packet. For this reason, these coefficients are treated empirically and extracted by fitting to experimental data.

An immediate consequence of Eq. (3) is that a time-resolved detection limited to a fixed point $(\bar{x},\bar{y})$ in the transverse plane yields a signal $S_{2D}(\bar{x},\bar{y},\tau)$ that mimics the conventional impulsive time-resolved signal undergoing some apparent shifts and distortions due to the temporal displacement $\Delta\tau$.

The space-dependent model of this Letter is examined by means of a simplified version of the standard experimental setup designed to study ultrafast Raman coherence in gases [16,17,33,34]. The simplification amounts to the use of one single femtosecond laser source and the replacement of the spectroscopic detection tools with an imaging system. The femtosecond pulses are thus degenerate but spectrally broad, with the two pump (or driving) electric fields derived from the same laser source, providing two distinct frequencies within its spectral bandwidth. A third laser field serves as the probe, reading the molecular coherence after a controlled delay. The key details of the experimental setup are outlined below.

The driving and reading pulses were generated by a Ti:Sapphire laser system (Coherent Hidra amplifier seeded by a Coherent Mantis oscillator), delivering transform-limited 50 fs pulses at 800 nm with an approximately Gaussian beam profile of 17 mm diameter. They were split into two parts of equal energy using a beam splitter. One of these was further divided by a secondary beam splitter with 20% transmission. The reflected portion was directed through another beam splitter, producing two synchronous excitation pulses driving the Raman coherence. The transmitted pulse (probe) was routed through a translation stage to probe Raman coherence at specific time delays. All pulses were focused using a lens with a 55-cm focal length in a three-dimensional phase-matching configuration as shown in Fig. 1(a) (folded BOXCARS).

The pulse energies, varied within the range of tens of μJ, were used to generate Raman coherence in air under ambient pressure conditions and at temperatures up to 600 °C. Temperature control during the experiments was achieved using a controlled heating source (heat gun), with measurements monitored via a K-type thermocouple. Signal collimation was achieved using a lens with a 20-cm focal length. The three-dimensional pulse geometry

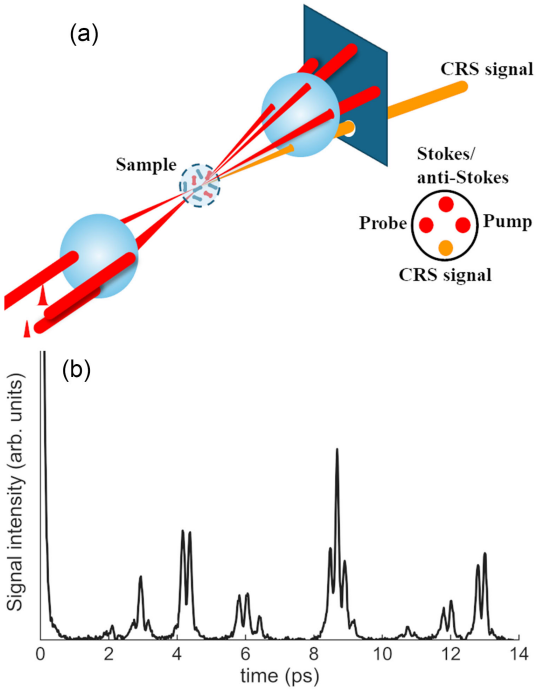

FIG. 1. (a) Three-dimensional phase-matching geometry and (b) typical detected time trace as for a conventional time-resolved approach.

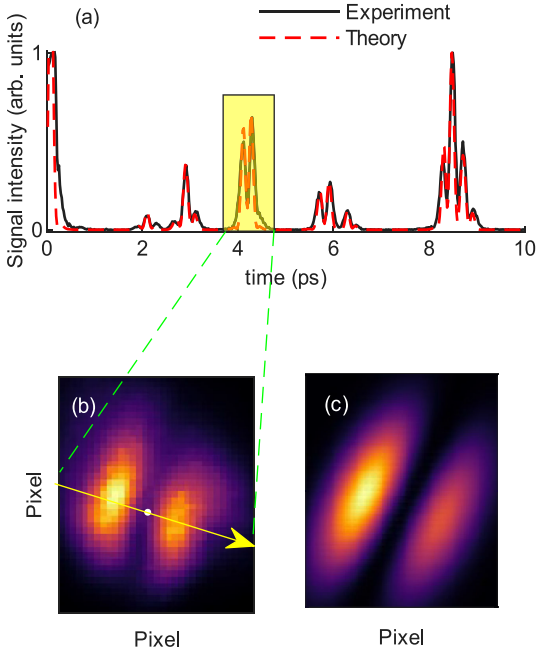

FIG. 2. (a) Experimental time trace (solid black line) extracted from the highlighted pixel (white dot) of the image in (b) and corresponding simulated trace (dashed red line). (b) Experimental image of the spatial signal observed at the time delay of 4.19 ps. The image is made of 33×41 pixels, each covering an effective temporal surface of about 20×20 fs^2 after conversion of the CCD area into time as detailed in Ref. [42]. The yellow arrow shows the direction of the effective time axis defined by the propagation direction of the polarization wave shown in the video available as Supplemental Material [22]. The whole arrow covers in space the highlighted window of the time traces in (a). (c) Simulation of the experimental image.

effectively isolated the CRS signal within the cone illuminated by the phase-matched radiation from nitrogen and oxygen molecules.

The signal was captured using a thermoelectrically cooled, back-illuminated CCD camera (Newton 940, Andor-Oxford Instruments) at the distance of approximately 60 cm from the probe volume. Selecting a restricted pixel area on the camera allowed the coherent signal evolution to be tracked as the delay progressed, mimicking conventional time-resolved approaches [17,33–39]. To achieve a recording frame rate of 10 Hz that matched the laser repetition rate, an 8×8 binning was performed on the CCD chip. Conventional time-resolved measurements were conducted by isolating a small region of the CCD chip. An example is shown in Fig. 1(b). The collapses and revivals of the rotational wave packet were distinctly observed at the expected delays, corresponding to fractional values of the full revival time of $1/(2Bc)$ where B is the rotational constant [40]. Two sets of fractional revivals are thus recognizable in Fig. 1(b). For nitrogen, the full revival occurs at approximately $\tau_{N_2} \cong 8.38$ ps, and, reflecting the rotational dynamics during the free evolution of the Raman coherence, fractional revivals at $\tau_{N_2}/4 \cong 2.09$ ps, $\tau_{N_2}/2 \cong 4.19$ ps, and $3\tau_{N_2}/4 \cong 6.28$ ps are also detected. Similarly, for oxygen, the full revival occurs at $\tau_{O_2} \cong 11.59$ ps with fractional revivals appearing at $\tau_{O_2}/4 \cong 2.90$ ps, $\tau_{O_2}/2 \cong 5.80$ ps, and $3\tau_{O_2}/4 \cong 8.69$ ps. In the following, we focus our analysis on the N_2 half revival, which serves as the representative case study of a molecular rotor whose wave packet is well characterized [41].

As discussed earlier, measuring the time trace captures the temporal component of phase coherence while keeping the spatial phase fixed. This behavior is illustrated in Fig. 2(a), where the trace represents the signal recorded at a specific pixel of about 100×100 μm^2 on the CCD [indicated by the white spot in Fig. 2(b)]. Changing the relative polarization angles of the linearly polarized laser pulses was of no consequence, except for a general decrease in signal intensity. The theoretical reconstruction of the time trace is also shown in Fig. 2(a), with details of the simulation method available in the Supplemental Material [22].

The comparison between the highlighted region of Fig. 2(a) and the image of Fig. 2(b) recorded at ~4.19 ps delay reveals that the spatial phase serves as a carrier of both past and future time-resolved spectroscopic information. In Fig. 2(b), each pixel is mapped onto time (about 20×20 fs^2 per pixel) on the basis of the effective time direction (yellow arrow) defined by the propagation direction of the polarization wave. Its motion is captured at

multiple time delays whose ordered sequence forms the video provided as Supplemental Material [22]. The correspondence between temporal and spatial information resulting from our approach underscores the potential of spatial phase coherence to facilitate single-shot measurements, which are traditionally accomplished at a fixed delay using more intricate experimental setups, such as the chirped-probe technique [43] or other phase-engineered approaches [39].

Figure 2(c) presents a theoretical reconstruction of the spatial signal generated under the Gaussian approximation for the temporal and spatial profiles of the laser pulses, revealing several key features [the theoretical explanation for Fig. 2(c) can be found in the Supplemental Material [22]]. Most notably, the spots appear elongated at an angle of approximately 70 degrees as dictated by the wave vector mixing (phase matching) projected onto the transverse plane. The manner in which the physics of the experimental geometry maps spatial coordinates onto the CCD is discussed in a dedicated numerical study [42]. Phase matching also drives the transformation of the originally Gaussian profile into the observed elliptical shape of the illuminated region.

The distinctive features of spatial phase measurements are demonstrated in the video provided in the Supplemental Material [22]. The video showcases a sequence of images, similar to Fig. 2(b), captured at larger time delays. These images replicate the structure of conventional time traces while offering more detailed insights into the evolution of the phase in both its temporal and spatial components. This further highlights the technique's potential for enabling single-shot measurements.

Another key phenomenon that links spatial and temporal phase components is captured in Fig. 3, where two experimental time frames of the half revival of nitrogen are compared in Figs. 3(a) and 3(b). The images are collected at two distinct delays whose time separation is 100 fs corresponding to the time required for the quantum-mechanical angular distribution of the rotational wave packet to evolve across one of the two extreme configurations (i.e., prolate and oblate) that characterize the signal maxima [41]. Thus, the temporal separation of 100 fs is sufficient to reveal a redistribution of the spatial coherence that generates the transverse propagation of the macroscopic polarization wave. The outcome is the shift of the peak signal intensity observed in Figs. 3(a) and 3(b). This means that this short time is enough to observe a redistribution of the spatial phase accompanying the macroscopic (semiclassical) propagation of the polarization wave.

The simulated images in Figs. 3(c) and 3(d) successfully replicate this phenomenon, providing further evidence of the dynamic relationship between spatial and time coordinates.

An important implication of these observations concerns purely time-resolved measurements. Without careful spatial

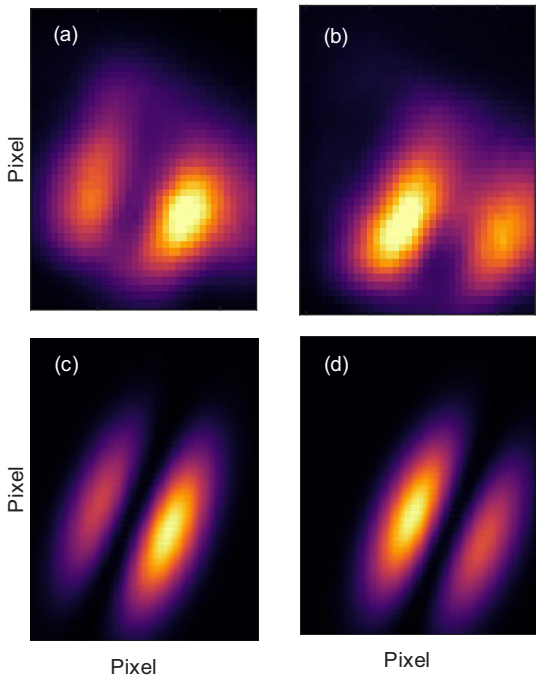

FIG. 3. Experimental images (a) and (b) of the nitrogen half revival captured at two delays separated by 100 fs. The more intense signal swings from one peak to the other as the delay increases or decreases. The simulation in the corresponding images (c) and (d) confirms the phenomenon.

selection, a signal recorded at a fixed nominal time delay can contain contributions from different temporal phases, arising from the conversion of spatial separation among molecules into an effective time delay. This mixing of spatiotemporal phases inevitably degrades the time resolution [44]. Based on this evidence, we highlight the critical importance of spatially resolved detection for accurate time-resolved measurements.

Sensitivity to the spatial phase was further examined by analyzing signals from various regions within the CCD photoactive plane. Figure 4 provides a comprehensive illustration of this sensitivity to the choice of regions where the time-resolved signal is measured across increasing delays. Below, we limit ourselves to examining the case of very small regions (single pixels). Additional details on measurements conducted using horizontal and vertical slits can be found in Fig. SM3 of the Supplemental Material [22].

The experimental time traces in Fig. 4(a) represent measurements taken from two specific pixels, labeled as points A and B in Fig. 4(b). This image reproduces the spatial distribution of the half revival of nitrogen at 4.16 ps delay. When the observation point changes, such as from A to B, a clear temporal phase shift appears in the time trace shown in Fig. 4(a). A simulated time trace that is independent of spatial effects is also shown in Fig. 4(a) as a solid black curve. Understandably, the temporal discrepancy between the experimental traces arises from the change in the spatial phase between the two selected points.

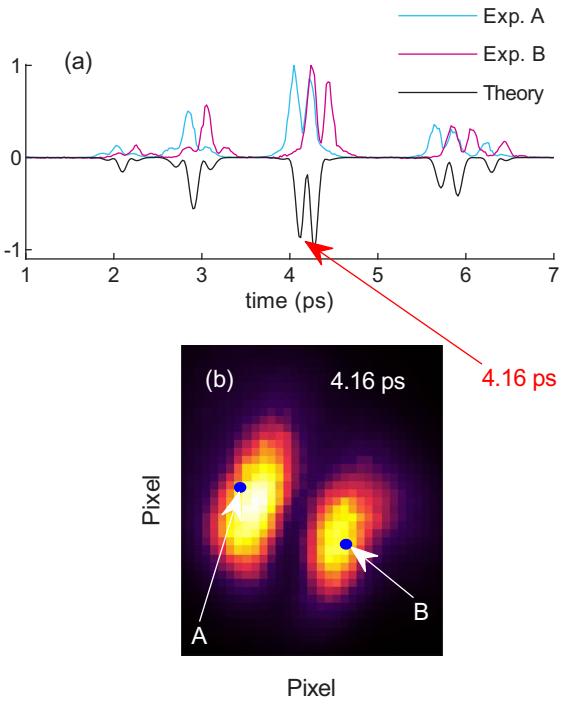

FIG. 4. (a) Experimental time traces (blue and red lines) measured at the selected pixels *A* and *B* in the image. The theoretical trace (black line) is also plotted. (b) Spatial distribution of the signal measured when the delay was 4.16 ps.

These findings have important implications for molecular alignment studies [21,37], particularly for manipulating and controlling the rotational states of molecules [45]. Such studies often rely on tightly focusing the signal onto a photodetector, which typically overlooks the temporal and spatial phase differences demonstrated in Fig. 4. Accounting for these effects could enhance the precision and understanding of molecular alignment experiments. Furthermore, the challenges in accurately determining the probe delay may stem from uncertainties related to the spatial selection of the observation region. This issue is frequently avoided by treating the delay as a fitting parameter, allowing it to vary freely over a range of several hundred femtoseconds [39,41].

An additional application of the proposed CRS technique is thermometry [10,16,17,34,36–39,43,46]. Raveesh *et al.* recently investigated the use of femtosecond rotational CARS for time-domain thermometry [47]. Their results showed that the shape of individual rotational revivals is highly sensitive to temperature, indicating that the ratio of signals from two closely delayed probe pulses (separated by tens of femtoseconds) within a revival could provide a sensitive measurement of temperatures. However, their experimental implementation encountered several challenges, likely arising from unaccounted spatial phase effects and transverse signal averaging, which introduced complications in the measurements.

The limitations identified in Ref. [47] can be overcome using the approach developed in the present Letter, in which CCD images are employed to extract time-resolved revival shapes while explicitly accounting for the spatial phase at any selected delay. Focusing on the half revival of nitrogen, the importance of spatial phase for thermometric measurements performed on a single laser shot basis is demonstrated in Fig. SM4 available as Supplemental Material [22]. This shows how the relative intensity of the two peaks within the revival varies when measured in a thermometrically controlled volume of air. The experimental results are further compared with simulations, showing good agreement.

In conclusion, our findings emphasize that a complete understanding of ultrafast Raman coherence must incorporate spatial information. Using Raman coherence of gaseous molecules interacting with femtosecond laser pulses as a case study, we identified limitations in the accuracy of conventional time-resolved measurements.

Notably, we observed a novel phenomenon, the "intensity swing," which involves a temporal shift of the maximum third-order response between peaks within the same revival. Recognizing this effect could significantly improve the precision of Raman coherence measurements. Additionally, we highlighted the potential for single-shot thermometry.

This Letter paves the way for new techniques in femtosecond laser spectroscopy, offering promising avenues. These include the development of a new type of Raman coherence imaging and the capability to quantify molecular species by means of the interference arising from overlapping fractional revivals in single-shot recordings. These advancements and their implications will be addressed in a forthcoming publication.

A final comment regards the practical extensions to vibrational CRS spectroscopy that is common for heavy gas molecules [48] or molecular constituents in soft and condensed matter [49,50]. For the latter, typical dephasing times are on the order of a few picoseconds, and advanced spectroscopic techniques are employed. These include temporal phase engineering to suppress the nonresonant background [51] or finding a balance between resolution, signal strength, and background interference [15]. Exploring spatial phase effects presents an intriguing alternative, provided the time-modulated signal exhibits sufficient contrast. This consideration is also relevant for single-molecule vibrational studies [52].

Acknowledgments—This study was funded by the Deutsche Forschungsgemeinschaft (DFG, German Research Foundation) under Germany's Excellence Strategy—Cluster of Excellence 2186, The Fuel Science Center"—ID No. 390919832, and also was performed within the Italian project "RICERCA E SVILUPPO DI TECNOLOGIE PER LA FILIERA DELL'IDROGENO POR-H2" ("Research and Development of Technologies for Hydrogen Chain," No. POR-H2, No. WP2, and

No. LA2.2.5), funded by the European Union (NextGenerationEU) through the Italian Ministry of Environment and Energy Security, under the National Recovery and Resilience Plan (PNRR, Mission 2, Component 2, Investment 3.5, Project Code No. I83C22001170006).

Data availability—The data that support the findings of this article are not publicly available upon publication because it is not technically feasible and/or the cost of preparing, depositing, and hosting the data would be prohibitive within the terms of this research project. The data are available from the authors upon reasonable request.

[1] V. L. Ginzburg and L. D. Landau, On the theory of superconductivity, Zh. Eksp. Teor. Fiz. **20**, 1064 (1950); Reprinted in Collected Papers of L. D. Landau (Pergamon Press, Oxford, 1965), 10.1016/C2013-0-01806-3.

[2] A. L. Schawlow and C. H. Townes, Infrared and optical masers, Phys. Rev. **112**, 1940 (1958).

[3] T. H. Maiman, Stimulated optical radiation in ruby, Nature (London) **187**, 493 (1960).

[4] R. J. Glauber, The quantum theory of optical coherence, Phys. Rev. **130**, 2529 (1963).

[5] A. T. Winfree, Biological rhythms and the behavior of populations of coupled oscillators, J. Theor. Biol. **16**, 15 (1967).

[6] M. Büttiker, Four-terminal phase-coherent conductance, Phys. Rev. Lett. **57**, 1761 (1986).

[7] A. Abramovici *et al.*, LIGO: The laser interferometer gravitational-wave observatory, Science **256**, 325 (1992).

[8] L. Mandel and E. Wolf, *Optical Coherence and Quantum Optics* (Cambridge University Press, New York, 1995).

[9] S. Mukamel, *Principles of Nonlinear Optical Spectroscopy* (Oxford University Press, New York, 1995).

[10] A. C. Eckbreth, *Laser Diagnostics for Combustion Temperature and Species* (Gordon and Breach Publishers, Amsterdam, 1996).

[11] J. D. Schultz *et al.*, Coherence in chemistry: Foundations and frontiers, Chem. Rev. **124**, 11641 (2024).

[12] J. D. Monnier, Optical interferometry in astronomy, Rep. Prog. Phys. **66**, 789 (2003).

[13] F. Dalfovo, S. Giorgini, L. P. Pitaevskii, and S. Stringari, Theory of Bose-Einstein condensation in trapped gases, Rev. Mod. Phys. **71**, 463 (1999).

[14] A. Zumbusch, G. R. Holtom, and X. S. Xie, Three-dimensional vibrational imaging by coherent anti-Stokes Raman scattering, Phys. Rev. Lett. **82**, 4142 (1999).

[15] D. Pestov *et al.*, Optimizing the laser-pulse configuration for coherent Raman spectroscopy, Science **316**, 265 (2007).

[16] S. Roy, J. R. Gord, and A. Patnaik, Recent advances in coherent anti-Stokes Raman scattering spectroscopy: Fundamental developments and applications in reacting flows, Prog. Energy Combust. Sci. **36**, 280 (2010).

[17] H. U. Stauffer, J. D. Miller, M. N. Slipchenko, T. R. Meyer, B. D. Prince, S. Roy, and J. R. Gord, Time- and frequency-dependent model of time-resolved coherent anti-Stokes Raman scattering (CARS) with a picosecond-duration probe pulse, J. Chem. Phys. **140**, 024316 (2014).

[18] C. H. Camp Jr and M. T. Cicerone, Chemically sensitive bioimaging with coherent Raman scattering, Nat. Photonics **9**, 295 (2015).

[19] D. R. Dietze and R. A. Mathies, Femtosecond stimulates Raman spectroscopy, Chem. Phys. Chem. **17**, 1224 (2016).

[20] R. Righini, Ultrafast optical Kerr effect in liquids and solids, Science **262**, 1386 (1993).

[21] H. Stapelfeldt and T. Seideman, Aligning molecules with strong laser pulses, Rev. Mod. Phys. **75**, 543 (2003).

[22] See Supplemental Material at http://link.aps.org/supplemental/10.1103/r98z-7bwj for detailed description of the simulation, as well as effects of slits on signal sampling, and possible applications for thermometry, which includes Refs. [23–32].

[23] R. Bluhm, V. A. Kostelecký, and J. A. Porter, The evolution and revival structure of localized quantum wave packets, Am. J. Phys. **64**, 944 (1996).

[24] J.-F. Ripoche, G. Grillon, B. Prade, M. Franco, E. Nibbering, R. Lange, and A. Mysyrowicz, Determination of the time dependence of n2 in air, Opt. Commun. **135**, 310 (1997).

[25] I. Sh. Averbukh and N. F. Perelman, Fractional revivals: Universality in the long-term evolution of quantum wave packets beyond the correspondence principle dynamics, Phys. Lett. A **139**, 449 (1989).

[26] M. Raveesh, A. Dominguez, M. Linne, J. Bood, and A. Hosseinnia, Interferometric quantum control (IQC) by fs/ns rotational coherent anti-Stokes Raman spectroscopy (RCARS), Opt. Express **31**, 38064 (2023).

[27] L. Martnisson, P.-E. Bengtsson, M. Aldén, and S. Kröll, A test of different rotational Raman linewidth models: Accuracy of rotational coherent anti-Stokes Raman scattering thermometry in nitrogen from 295 to 1850 K, J. Chem. Phys. **99**, 2466 (1993).

[28] A. Bohlin, P.-E. Bengtsson, and M. Marrocco, On the sensitivity of rotational CARS N2 thermometry to the Herman-Wallis factor, J. Raman Spectrosc. **42**, 1843 (2011).

[29] A. Bohlin, E. Nordström, P.-E. Bengtsson, and M. Marrocco, On the sensitivity of rotational CARS O2 thermometry to the Herman-Wallis factor, J. Raman Spectrosc. **43**, 599 (2012).

[30] L. Martnisson, P.-E. Bengtsson, and M. Aldén, Oxygen concentration and temperature measurements in N2-O2 mixtures using rotational coherent anti-Stokes Raman spectroscopy, Appl. Phys. B **62**, 29 (1996).

[31] M. Marrocco, Time-domain coherent anti-Stokes Raman scattering in terms of the time-delayed Yuratich equation, Opt. Lett. **39**, 4831 (2014).

[32] T. Vieillard, F. Chaussard, F. Billard, D. Sugny, O. Faucher, S. Ivanov, J. M. Hartmann, C. Boulet, and B. Lavorel, Field-free molecular alignment for probing collisional relaxation dynamics, Phys. Rev. A **87**, 023409 (2013).

[33] M. Schmitt, G. Knopp, A. Materny, and W. Kiefer, The application of femtosecond time-resolved coherent anti-Stokes Raman scattering for the investigation of ground and excited state molecular dynamics of molecules in the gas phase, J. Phys. Chem. A **102**, 4059 (1998).

[34] H.-M. Frey, P. Beaud, T. Gerber, B. Mischler, P. P. Radi, and A. P. Tzannis, Femtosecond nonresonant degenerate four-wave mixing at atmospheric pressure and in a free jet, Appl. Phys. B **68**, 735 (1999).
[35] T. Lang, K.-L. Kompa, and M. Motzkus, Femtosecond CARS on H2, Chem. Phys. Lett. **310**, 65 (1999).
[36] P. Beaud, H.-M. Frey, T. Lang, and M. Motzkus, Flame thermometry by femtosecond CARS, Chem. Phys. Lett. **344**, 407 (2001).
[37] V. Renard, M. Renard, S. Guerin, Y. T. Pashayan, B. Lavorel, O. Faucher, and H. R. Jauslin, Postpulse molecular alignment measured by a weak field polarization technique, Phys. Rev. Lett. **90**, 153601 (2003).
[38] F. Chaussard, B. Lavorel, E. Hertz, and O. Faucher, Optical diagnostics with ultrafast and strong field Raman techniques, in *Ultrafast Phenomena in Molecular Sciences*, edited by R. de Nalda and L. Bañares (Springer, Heidelberg, 2014), Chap. 11.
[39] S. P. Kearney, Hybrid fs/ps rotational CARS temperature and oxygen measurements in the product gases of canonical flat flames, Combust. Flame **162**, 1748 (2015).
[40] R. W. Robinett, Quantum wave packet revivals, Phys. Rep. **392**, 1 (2004).
[41] J. Yang *et al.*, Diffractive imaging of a rotational wavepacket in nitrogen molecules with femtosecond megaelectronvolt electron pulses, Nat. Commun. **7**, 11232 (2016).
[42] F. Vergari, F. Mazza, M. Marrocco, and A. Hosseinnia, Geometrical control of spatio–temporal coherence in femtosecond rotational coherent Raman scattering, Opt. Lett. **51**, 604 (2026).
[43] D. R. Richardson, R. P. Lucht, W. D. Kulatilaka, S. Roy, and J. R. Gord, Theoretical modeling of single-laser-shot, chirped-probe-pulse femtosecond coherent anti-Stokes Raman scattering thermometry, Appl. Phys. B **104**, 699 (2011).
[44] B. Lavorel, O. Faucher, M. Morgen, and R. Chaux, Analysis of femtosecond Raman-induced polarization spectroscopy (RIPS) in N_2 and CO_2 by fitting and scaling laws, J. Raman Spectrosc. **31**, 77 (2000).
[45] A. Hosseinnia, M. Raveesh, A. Dominguez, M. Ruchkina, M. Linne, and J. Bood, Single-shot coherent control of molecular rotation by fs/ns rotational coherent anti-Stokes Raman spectroscopy, Opt. Express **30**, 32204 (2022).
[46] G. Batignani, E. Mai, M. Martinati, M. M. Neethish, S. Mukamel, and T. Scopigno, Temperature dependence of coherent versus spontaneous Raman scattering, Phys. Rev. Lett. **133**, 206902 (2024).
[47] M. Raveesh, A. Hosseinnia, A. Padhiary, X. Wei, V. Kornienko, E. Kristensson, A. Ehn, B. Peterson, M. Linne, and J. Bood, Exploring time-domain femtosecond rotational coherent Raman scattering for diagnostics, J. Raman Spectrosc. **56**, 666 (2025).
[48] C. C. Hayden and D. W. Chandler, Femtosecond time-resolved studies of coherent vibrational Raman scattering in large gas-phase molecules, J. Chem. Phys. **103**, 10465 (1995).
[49] L. Dhar, J. A. Rogers, and K. A. Nelson, Time-resolved vibrational spectroscopy in the impulsive limit, Chem. Rev. **94**, 157 (1994).
[50] A. Volkmer, L. D. Book, and X. S. Xie, Time-resolved coherent anti-Stokes Raman scattering microscopy: Imaging based on Raman free induction decay, Appl. Phys. Lett. **80**, 1505 (2002).
[51] D. Oron, N. Dudovich, and Y. Silberberg, Femtosecond phase-and-polarization control for background-free coherent anti-Stokes Raman spectroscopy, Phys. Rev. Lett. **90**, 213902 (2003).
[52] S. Yampolsky, D. A. Fishman, S. Dey, E. Hulkko, M. Banik, E. O. Potma, and V. A. Apkarian, Seeing a single molecule vibrate through time-resolved coherent anti-Stokes Raman scattering, Nat. Photonics **8**, 650 (2014).